A Comparison of Nonlinear PI and PID Inertia-Free Spacecraft Attitude Control Laws

Marc Camblor[2], Avishai Weiss[1], Gerardo Cruz[1],
Yousaf Rahman[1], Sergio Esteban[2],
Ilya V. Kolmanovsky[1], and Dennis S. Bernstein[1]

[1] Department of Aerospace Engineering, University of Michigan, Ann Arbor, MI 48109-2140, USA
{avishai,gecruz,yousafrm,ilya,dsbaero}@umich.com
[2] Department of Aerospace Engineering, Universidad de Sevilla, 41092 Sevilla, Spain
marcamchi@alumn.us.es, sesteban@us.es

Abstract. We compare four spacecraft attitude control laws that require no prior modeling of the spacecraft mass distribution. All four control laws are based on rotation matrices, which provide a singularity-free attitude representation and unwinding-free operation without discontinuous switching. We apply these control laws to motion-to-rest and motion-to-spin maneuvers. Simulation results are given to illustrate the robustness of the control laws to uncertainty in the spacecraft inertia. For motion-to-rest maneuvers about a principal axis with bounded torque, we compare the settling time of the inertia-free control laws with the time-optimal bang-bang control law operating under known inertia. We also investigate closed-loop performance in the presence of attitude-dependent torque disturbances, actuator nonlinearities, sensor noise, and actuator bias.

Keywords: Attitude control, unmodeled inertia, rotation matrix, SO(3).

1 Introduction

The development of a spacecraft attitude control system is often a labor-intensive process due to the need for an accurate model of the spacecraft inertia. Determining and predicting the mass properties of a spacecraft may be difficult due to fuel usage, deployment, structural articulation, and docking. To alleviate this need, this paper focuses on spacecraft attitude control laws that require no modeling of the spacecraft's mass distribution. An adaptive inertia-free attitude control law is given in [1] for minimum-time maneuvers. Inertia-free control laws for motion-to-rest and tracking are given in [2–4].

Attitude control laws can use various parameterizations of the rotation group SO(3). Euler angles are conceptually the simplest, but cannot represent all angular velocities due to singularities corresponding to gimbal lock. A related obstacle arises in the use of Rodrigues parameters and modified Rodrigues parameters,

D. Choukroun et al. (eds.), *Advances in Estimation, Navigation, and Spacecraft Control*,
DOI: 10.1007/978-3-662-44785-7_27

which have singularities at 180-deg and 360-deg rotation angles, respectively. The most common attitude representation is based on quaternions, which can represent all attitudes and all angular velocities, but provide a double cover of SO(3), that is, each physical attitude is represented by two elements of the 4-dimensional sphere S^3. A continuous controller designed on the set of quaternions can thus inadvertently command the spacecraft to needlessly rotate 360 degrees to reach the commanded attitude. This is the unwinding problem [5]. The inertia-free, quaternion-based control laws in [3, 6, 7] exhibit unwinding.

There are several approaches to avoiding unwinding. The traditional approach is to implement a logic statement that confines the quaternions to a hemisphere of S^3 [8]. This approach introduces a discontinuous control law, which can lead to chattering in the presence of noise. This issue and associated complications are addressed in [9].

In the present paper we avoid unwinding by representing attitude in terms of rotation matrices, which constitute a one-to-one representation of physical attitude without attitude or angular-velocity singularities [10]. Attitude control on SO(3) thus provides the ability to implement continuous control laws that do not exhibit unwinding [11–13]. Inertia-free control laws on SO(3) are developed in [14, 15]. Lie groups are used for control in [16].

Since SO(3) is a compact manifold, every continuous vector field on it necessarily possesses more than one equilibrium, in fact, at least four. This means that global convergence on SO(3) under continuous, time-invariant control is impossible. Consequently, the objective of [12, 13, 15] is almost global stabilization, where the spurious equilibria are saddle points. Although the spurious equilibria can slow the rate of convergence, this approach avoids the complications of discontinuous control laws.

Although the derivation of the inertia-free controller in [15] and the present paper is based on rotation matrices, the attitude error given by the S-parameter defined by (7) can be computed from any attitude parameterization, such as quaternions or modified Rodrigues parameters, and thus these results are not confined to rotation matrices per se.

The goal of this paper is to compare four continuous, inertia-free attitude control laws based on rotation matrices. These control laws are called SO(3)/0, SO(3)/3, SO(3)/6, and SO(3)/9, where the last number represents the number of integrators in the control law. These control laws take the form of nonlinear PD/PID control laws tailored to the nonlinear characteristics of spacecraft dynamics. Since linearized rigid-body dynamics comprise a double integrator about each principal axis, we expect (as in the case of linear systems) that asymptotic tracking of attitude ramp commands (that is, spin commands) about each principal axis is possible without integral action. The primary role of integral control in spacecraft attitude dynamics is thus to reject constant disturbances.

In the simplest case of PD control, the inertia-free SO(3)/0 control law is given in [14]. In contrast, the SO(3)/9 control given in [15] is also inertia free but employs three integrators inside the feedback loop as well as six integrators for inertia estimation. The control laws SO(3)/3 and SO(3)/6 are ad hoc

simplifications of SO(3)/9. The goal of this paper is to numerically investigate and compare the closed-loop performance of these control laws under various command-following and disturbance-rejection scenarios as well as under various off-nominal conditions involving rate-sensor noise and unmodeled actuator nonlinearities, such as saturation, on-off, and deadzone.

We consider two basic scenarios, namely, motion-to-rest (M2R) maneuvers and motion-to-spin (M2S) maneuvers, where "rest" and "spin" refer to motion relative to an inertial frame. If the M2R and M2S maneuvers begin from zero angular velocity, then we use the terminology rest-to-rest (R2R) and rest-to-spin (R2S), respectively. A M2S maneuver aims to bring the spacecraft from an arbitrary initial angular velocity and attitude to a specified constant angular velocity relative to an inertial frame. In other words, the goal is to have the spacecraft rotate at a constant rate about a body-fixed axis whose inertial direction is fixed.

Although the spacecraft inertia is unknown, and thus the directions of the principal axes of inertia are unknown, we consider commanded spins about both principal and non-principal axes (without knowing whether the commanded axis of rotation is principal or non-principal) in order to demonstrate how these control laws perform in various scenarios. For example, a commanded spin about a principal axis has the advantage that, once the spacecraft reaches the commanded spin, no additional torque is needed in the absence of disturbances except possibly to stabilize a spin about the minimum and intermediate axes, where the latter is naturally unstable and the former is unstable due to energy dissipation, although we do not model this effect. Furthermore, as shown in [17, p. 377], a spin about a non-principal axis with constant torque and for which all components of the angular velocity are nonzero is unstable and thus stabilization is required. Finally, a commanded spin about a non-principal axis requires constant, nonzero torques and thus is more sensitive to torque saturation than a commanded spin about a principal axis. In summary, a commanded spin about a non-principal axis places significantly higher demands on the control law in terms of stabilization and control authority.

Throughout this paper, all control torques are assumed to be provided by thrusters or gas jets without onboard stored momentum.

2 Spacecraft Model

The spacecraft equations of motion are given by Euler's and Poisson's equations

$$J\dot{\omega} = (J\omega) \times \omega + Bu + z_{\text{dist}}, \tag{1}$$

$$\dot{R} = R\omega^{\times}, \tag{2}$$

where $\omega \in \mathbb{R}^3$ is the angular velocity of the spacecraft frame relative to the inertial frame resolved in the spacecraft frame, $\omega^{\times}$ is the cross-product matrix of ω, $J \in \mathbb{R}^{3\times3}$ is the inertia matrix of the spacecraft, the components of the vector $u \in \mathbb{R}^3$ represent three independent torque inputs, and the nonsingular matrix $B \in \mathbb{R}^{3\times3}$ determines the applied torque about each axis of the spacecraft

frame due to u. The rotation matrix $R = \mathcal{O}_{\mathrm{In/SC}} \in \mathbb{R}^{3\times 3}$ is the physical rotation matrix that transforms the inertial frame into the spacecraft frame resolved in the spacecraft frame, and where $\mathcal{O}_{\mathrm{In/SC}}$ is the orientation (direction cosine) matrix that transforms components of a vector resolved in the spacecraft frame into the components of the same vector resolved in the inertial frame. The vector $z_{\mathrm{dist}} \in \mathbb{R}^3$ represents disturbance torques, such as the gravity gradient torques modeled by (25) below.

The objective of the attitude control problem is to determine control inputs such that the spacecraft attitude given by R follows a commanded attitude trajectory given by the possibly time-varying C^1 rotation matrix $R_{\mathrm{d}}(t)$. For $t \geq 0$, $R_{\mathrm{d}}(t)$ is given by

$$\dot{R}_{\mathrm{d}}(t) = R_{\mathrm{d}}(t)\omega_{\mathrm{d}}(t)^{\times}, \quad R_{\mathrm{d}}(0) = R_{\mathrm{d}0}, \tag{3}$$

where ω_{d} is the commanded possibly time-varying angular velocity vector resolved in the desired body frame specified by $R_{\mathrm{d}}(t)$. The error between $R(t)$ and $R_{\mathrm{d}}(t)$ is given by the attitude-error rotation matrix $\tilde{R} \triangleq R_{\mathrm{d}}^{\mathrm{T}} R$, which satisfies the differential equation $\dot{\tilde{R}} = \tilde{R}\tilde{\omega}^{\times}$, where the angular-velocity error $\tilde{\omega}$ is defined by $\tilde{\omega} \triangleq \omega - \tilde{R}^{\mathrm{T}}\omega_{\mathrm{d}}$. We rewrite (1) in terms of $\tilde{\omega}$ as

$$J\dot{\tilde{\omega}} = J(\tilde{\omega} + \tilde{R}^{\mathrm{T}}\omega_{\mathrm{d}}) \times (\tilde{\omega} + \tilde{R}^{\mathrm{T}}\omega_{\mathrm{d}}) + J(\tilde{\omega} \times \tilde{R}^{\mathrm{T}}\omega_{\mathrm{d}} - \tilde{R}^{\mathrm{T}}\dot{\omega}_{\mathrm{d}}) + Bu + z_{\mathrm{dist}}. \tag{4}$$

A scalar measure of attitude error is given by the eigenaxis error

$$e(t) \triangleq \cos^{-1}(\tfrac{1}{2}[\mathrm{tr}\,\tilde{R}(t) - 1]).$$

3 Control Laws

3.1 SO(3)/9

To estimate the spacecraft inertia, we introduce the notation $J\omega = L(\omega)\gamma$, where $\gamma \in \mathbb{R}^6$ is defined by

$$\gamma \triangleq \begin{bmatrix} J_{11} & J_{22} & J_{33} & J_{23} & J_{13} & J_{12} \end{bmatrix}^{\mathrm{T}} \tag{5}$$

and

$$L(\omega) \triangleq \begin{bmatrix} \omega_1 & 0 & 0 & 0 & \omega_3 & \omega_2 \\ 0 & \omega_2 & 0 & \omega_3 & 0 & \omega_1 \\ 0 & 0 & \omega_3 & \omega_2 & \omega_1 & 0 \end{bmatrix}.$$

Next, let $\hat{J} \in \mathbb{R}^{3\times 3}$ denote an estimate of J, and define the inertia-estimation error $\tilde{J} \triangleq J - \hat{J}$. Letting $\hat{\gamma}, \tilde{\gamma} \in \mathbb{R}^6$ represent $\hat{J}, \tilde{J}$, respectively, as in (5), it follows that $\tilde{\gamma} = \gamma - \hat{\gamma}$. Likewise, let $\hat{z}_{\mathrm{dist}} \in \mathbb{R}^3$ denote an estimate of z_{dist}, and define the disturbance-estimation error $\tilde{z}_{\mathrm{dist}} \triangleq z_{\mathrm{dist}} - \hat{z}_{\mathrm{dist}}$.

Assuming that the disturbance is harmonic, z_{dist} can be modeled by

$$\dot{d} = A_{\text{dist}} d, \quad z_{\text{dist}} = C_{\text{dist}} d, \tag{6}$$

where $A_{\text{dist}} \in \mathbb{R}^{n_d \times n_d}$ and $C_{\text{dist}} \in \mathbb{R}^{3 \times n_d}$ are known matrices. In this model, $d(0)$ is unknown, which is equivalent to the assumption that the amplitude and phase of all harmonic components in the disturbance are unknown; however, the spectrum of d is assumed to be known. To provide asymptotic rejection of harmonic disturbances, the matrix A_{dist} is chosen to include eigenvalues of all frequency components that may be present in z_{dist}, where the zero eigenvalue corresponds to a constant disturbance. Since z_{dist} is harmonic, A_{dist} is chosen to be skew symmetric. Let $\hat{d} \in \mathbb{R}^{n_d}$ denote an estimate of d, and define the disturbance-state estimation error $\tilde{d} \triangleq d - \hat{d}$.

The role of $\text{tr}(A - A\tilde{R})$ in the stability analysis below is explained by the following result.

Lemma 1. [15] Let $A \in \mathbb{R}^{3\times3}$ be a diagonal positive-definite matrix, and let R be a rotation matrix. Then, the following statements hold:

i) For all $i, j = 1, 2, 3$, $R_{ij} \in [-1, 1]$.
ii) $\text{tr}(A - AR) \geq 0$.
iii) $\text{tr}(A - AR) = 0$ if and only if $R = I$.

The attitude error S is defined by [11, 13–15]

$$S \triangleq \sum_{i=1}^{3} a_i (\tilde{R}^{\text{T}} e_i) \times e_i, \tag{7}$$

where a_1, a_2, a_3 are distinct positive numbers and $e_1, e_2, e_3 \in \mathbb{R}^3$ are the standard basis vectors.

Theorem 1. [15] Let K_{p} be a positive number, let $K_1 \in \mathbb{R}^{3\times3}$, $Q \in \mathbb{R}^{6\times6}$, and $D \in \mathbb{R}^{n_d \times n_d}$ be positive definite, let $A = \text{diag}(a_1, a_2, a_3)$ be a diagonal positive-definite matrix, and define the attitude error S by (7). Then the Lyapunov candidate

$$V(\tilde{\omega}, \tilde{R}, \tilde{\gamma}, \tilde{d}) \triangleq \tfrac{1}{2}(\tilde{\omega} + K_1 S)^{\text{T}} J (\tilde{\omega} + K_1 S) + K_{\text{p}} \text{tr}\,(A - A\tilde{R}) + \tfrac{1}{2}\tilde{\gamma}^{\text{T}} Q \tilde{\gamma} + \tfrac{1}{2}\tilde{d}^{\text{T}} D \tilde{d}$$

is positive definite, that is, V is nonnegative, and $V = 0$ if and only if $\tilde{\omega} = 0$, $\tilde{R} = I$, $\tilde{\gamma} = 0$, and $\tilde{d} = 0$.

Theorem 2. [15] Let K_{p} be a positive number, let $K_{\text{v}} \in \mathbb{R}^{3\times3}$, $K_1 \in \mathbb{R}^{3\times3}$, $Q \in \mathbb{R}^{6\times6}$, and $D \in \mathbb{R}^{n_d \times n_d}$ be positive definite, assume that $A_{\text{dist}}^{\text{T}} D + D A_{\text{dist}}$ is negative semidefinite, let $A = \text{diag}(a_1, a_2, a_3)$ be a diagonal positive-definite matrix with distinct diagonal entries, define S and V as in Theorem 1, and let $\hat{\gamma}$ and $\hat{d}$ satisfy

$$\dot{\hat{\gamma}} = Q^{-1}[L^{\text{T}}(\omega)\omega^{\times} + L^{\text{T}}(K_1 \dot{S} + \tilde{\omega} \times \omega - \tilde{R}^{\text{T}} \dot{\omega}_{\text{d}})](\tilde{\omega} + K_1 S), \tag{8}$$

where

$$\dot{S} = \sum_{i=1}^{3} a_i[(\tilde{R}^{\mathrm{T}} e_i) \times \tilde{\omega}] \times e_i, \tag{9}$$

and

$$\dot{\hat{d}} = A_{\mathrm{dist}}\hat{d} + D^{-1}C_{\mathrm{dist}}^{\mathrm{T}}(\tilde{\omega} + K_1 S), \quad \hat{z}_{\mathrm{dist}} = C_{\mathrm{dist}}\hat{d}. \tag{10}$$

Furthermore, let

$$u = B^{-1}(v_1 + v_2 + v_3), \tag{11}$$

where

$$v_1 \stackrel{\triangle}{=} -(\hat{J}\omega) \times \omega - \hat{J}(K_1\dot{S} + \tilde{\omega} \times \omega - \tilde{R}^{\mathrm{T}}\dot{\omega}_{\mathrm{d}}), \tag{12}$$

$$v_2 \stackrel{\triangle}{=} -\hat{z}_{\mathrm{dist}}, \quad v_3 \stackrel{\triangle}{=} -K_{\mathrm{p}}S - K_{\mathrm{v}}(\tilde{\omega} + K_1 S). \tag{13}$$

Then,

$$\begin{aligned}\dot{V}(\tilde{\omega}, \tilde{R}, \tilde{\gamma}, \tilde{d}) = &- (\tilde{\omega} + K_1 S)^{\mathrm{T}} K_{\mathrm{v}}(\tilde{\omega} + K_1 S) - K_{\mathrm{p}} S^{\mathrm{T}} K_1 S \\ &+ \tfrac{1}{2}\tilde{d}^{\mathrm{T}}(A_{\mathrm{dist}}^{\mathrm{T}} D + D A_{\mathrm{dist}})\tilde{d}\end{aligned} \tag{14}$$

is negative semidefinite. Furthermore, the equilibrium manifold $(\tilde{\omega}, \tilde{R}, (\tilde{\gamma}, \tilde{d})) = (0, I, \mathcal{Q}_0)$ of the closed-loop system given by (4) and (8)-(13) is locally asymptotically stable, and the remaining equilibrium manifolds given by $(0, \mathcal{R}_i, \mathcal{Q}_i)$, for $i \in \{1, 2, 3\}$ are unstable. Finally, the set of all initial conditions converging to these equilibrium manifolds forms a lower dimensional submanifold of $\mathbb{R}^3 \times \mathrm{SO}(3) \times \mathbb{R}^6 \times \mathbb{R}^3$.

Saturation techniques for SO(3)/9 are discussed in [18].

3.2 SO(3)/6

The control law SO(3)/6 is a simplification of the SO(3)/9 control law (11)–(13) with v_2 and thus (10) omitted. In particular, this control law has the form

$$u = -B^{-1}[(K_{\mathrm{p}}I + K_{\mathrm{v}}K_1)S + K_{\mathrm{v}}\tilde{\omega} + \hat{J}K_1\dot{S} + (\hat{J}\omega) \times \omega + \hat{J}(\tilde{\omega} \times \omega) - \hat{J}\tilde{R}^{\mathrm{T}}\dot{\omega}_{\mathrm{d}}]. \tag{15}$$

3.3 SO(3)/3

The control law SO(3)/3 is a simplification of the SO(3)/9 control law (11)–(13) with the inertia estimate (8) omitted and with $A_{\mathrm{dist}} = 0$. In particular, this control law has the form

$$u = -B^{-1}\left[(K_{\mathrm{p}}I + K_{\mathrm{v}}K_1)S + K_{\mathrm{i}}C_{\mathrm{dist}}D^{-1}C_{\mathrm{dist}}^{\mathrm{T}}\int_0^t [\tilde{\omega}(s) + K_1 S(s)]\,\mathrm{d}s + K_{\mathrm{v}}\tilde{\omega}\right], \tag{16}$$

where the integral gain K_{i} is a positive number.

3.4 SO(3)/0

The SO(3)/0 control law for almost global stabilization [14, 15] is given by

$$u = -B^{-1}(K_{\mathrm{p}} S + K_{\mathrm{v}} \tilde{\omega}), \tag{17}$$

where the positive number K_{p} and the positive-definite matrix $K_{\mathrm{v}} \in \mathbb{R}^{3\times 3}$ are proportional (attitude) and derivative (angular velocity) gains, respectively.

Note that the control law (17) is inertia-free. The stabilizing effect of this control law on the attitude of a rigid spacecraft follows from the Lyapunov function

$$V(\omega, \tilde{R}) \triangleq \tfrac{1}{2}\omega^{\mathrm{T}} J \omega + K_{\mathrm{p}} \mathrm{tr}(A - A\tilde{R}), \tag{18}$$

where $A \triangleq \mathrm{diag}(a_1, a_2, a_3)$ and for which $\dot{V}(\omega, \tilde{R}) = -\omega^{\mathrm{T}} K_{\mathrm{v}} \omega$. The invariant set theorem is used in [14] to ensure almost global asymptotic stability.

By choosing K_{v} to be a function of ω, the control law (17) satisfies the following saturation bounds [15, 18].

Proposition 1. Let α and β be positive numbers, let $A = \mathrm{diag}(a_1, a_2, a_3)$ have distinct positive diagonal entries, and let K_{p} and $K_{\mathrm{v}}(\omega)$ be given by

$$K_{\mathrm{p}} = \frac{\alpha}{\mathrm{tr}\, A} \tag{19}$$

and

$$K_{\mathrm{v}}(\omega) = \beta \begin{bmatrix} \frac{1}{1+|\omega_1|} & 0 & 0 \\ 0 & \frac{1}{1+|\omega_2|} & 0 \\ 0 & 0 & \frac{1}{1+|\omega_3|} \end{bmatrix}. \tag{20}$$

Then, for all $t \geq 0$, the control torque given by (17) satisfies

$$\|u(t)\|_\infty \leq \frac{\alpha + \beta}{\sigma_{\min}(B)}. \tag{21}$$

For the remainder of the paper, K_{p} and K_{v} are assumed to be given by (19) and (20). Alternative forms of the gain $K_{\mathrm{v}}(\omega)$ are given in [19].

4 Modeling Inertia Variations

If the inertia tensor is resolved in a non-principal body-fixed frame, then the diagonal entries of the resulting inertia matrix are the moments of inertia and the off-diagonal entries are the products of inertia. The off-diagonal entries of the inertia matrix are thus a consequence of an unknown rotation between a principal body-fixed frame and an arbitrarily chosen body-fixed frame.

Figure 1 shows the triangular region of feasible principal moments of inertia of a rigid body. There are five cases that are highlighted for the principal moments

of inertia $\lambda_1 \geq \lambda_2 \geq \lambda_3 > 0$, where $\lambda_1, \lambda_2, \lambda_3$ satisfy the triangle inequality $\lambda_1 < \lambda_2 + \lambda_3$. Let m denote the mass of the rigid body. The point $\lambda_1 = \lambda_2 = \lambda_3$ corresponds to a sphere of radius $\hat{r} = \sqrt{\frac{5\lambda_1}{2m}}$; the point $\lambda_1 = \lambda_2 = 2\lambda_3$ corresponds to a cylinder of length l and radius r, where $l = 3r$ and $r = \sqrt{\frac{2\lambda_1}{m}}$; and the point $\lambda_1 = \frac{6}{5}\lambda_2 = 2\lambda_3$ is a brick whose side lengths are l_1, l_2, l_2 and whose inertia is located at the centroid of the triangular region. The remaining two cases in Figure 1 are limiting cases. In particular, the thin disk is a cylinder with zero length, positive radius, and infinite density, while the thin cylinder is a cylinder with positive length, zero radius, and infinite density. Note that the inertia matrix of the thin disk is positive definite, whereas the inertia matrix of the thin cylinder is positive semidefinite but not positive definite. Table 1 summarizes the parameters and densities for each of these rigid bodies.

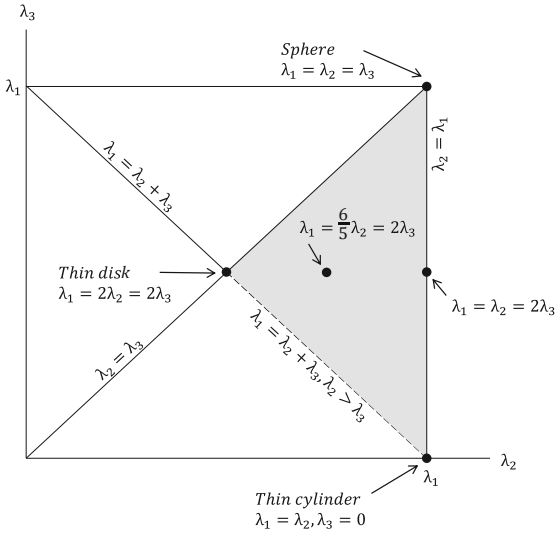

Fig. 1. Feasible region of the principal moments of inertia $\lambda_1, \lambda_2, \lambda_3$ of a rigid body satisfying $0 < \lambda_3 \leq \lambda_2 \leq \lambda_1$, where $\lambda_1 < \lambda_2 + \lambda_3$. The shaded region shows all feasible values of λ_2 and λ_3 in terms of the largest principal moment of inertia λ_1. The open dots and dashed line segment indicate nonphysical, limiting cases.

5 M2R Examples

For all of the examples in this section, we assume that the nominal body-fixed frame is a principal body-fixed frame. However, the body-fixed frame is not a principal-axis frame for the off-nominal cases considered below. The nominal spacecraft shape is chosen to be a brick corresponding to the centroid of the triangular region in Figure 1. For all cases considered, we choose $\lambda_1 = 10$ kg-m^2, which for the centroidal brick yields the inertia $J_3 = \text{diag}(10, 25/3, 5)$. Consequently, the inertias J_1, J_2, J_4, and J_5 of the sphere, cylinder, thin disk, and thin

Table 1. Parameters and densities for the inertia matrices considered in Figure 1. Note that the parameters for all shapes are set by the ratio λ_1/m, where λ_1 is the principal moment of inertia and m is the mass.

Shape	Parameters	Density
Sphere	$\hat{r} = \sqrt{\frac{5\lambda_1}{2m}}$	$\rho = \frac{4}{3}\pi m^{2/5}(\frac{5\lambda_1}{2})^{2/5}$
Cylinder	$l = 3r$, $r = \sqrt{\frac{2\lambda_1}{m}}$	$\rho = 3\pi m^{2/5}(2\lambda_1)^{2/5}$
Brick	$l_1 = \sqrt{\frac{2\lambda_1}{m}}$, $l_2 = \sqrt{\frac{4\lambda_1}{m}}$, $l_3 = \sqrt{\frac{8\lambda_1}{m}}$	$\rho = 8m^{2/5}\lambda_1^{2/5}$
Thin disk	$l = 0$, $r = \sqrt{\frac{2\lambda_1}{m}}$	$\rho = \infty$
Thin cylinder	$r = 0$, $l = \sqrt{\frac{12\lambda_1}{m}}$	$\rho = \infty$

cylinder are given, respectively, by $J_1 = \mathrm{diag}(10, 10, 10)$, $J_2 = \mathrm{diag}(10, 10, 5)$, $J_4 = \mathrm{diag}(10, 5, 5)$, and $J_5 = \mathrm{diag}(10, 10, 0.1)$, where all units are kg-m^2. The inertia matrix J_3 corresponding to the centroid of the inertia region serves as the nominal inertia matrix, while a perturbation $J(\alpha)$ of J_i in the direction of J_j has the form $J(\alpha) = (1-\alpha)J_i + \alpha J_j$, where $\alpha \in [0, 1]$ is the perturbation parameter. To facilitate numerical integration, J_5 is chosen to be a nonsingular approximation of the inertia of a thin cylinder.

For all examples in the remainder of the paper, let $\alpha = \beta = 1$, $K_1 = I_3$, $K_\mathrm{i} = 0.015$, $A = \mathrm{diag}(1, 2, 3)$, $\mathrm{B} = \mathrm{I}_3$, $\mathrm{C_{dist}} = \mathrm{I}_3$, $\mathrm{D} = \mathrm{I}_3$, and $\mathrm{Q} = \mathrm{I}_6$. Furthermore, K_p and K_v are defined in (19) and (20), respectively. To evaluate the performance for R2R examples, we use the settling-time metric

$$k_0 = \min_{k>100}\{k : \text{ for all } i \in \{1, \ldots, 100\}, e((k-i)T_\mathrm{s}) < 0.05\,\mathrm{rad}\}, \tag{22}$$

where k is the simulation step, T_s is the integration step size, and $e(kT_\mathrm{s})$ is the eigenaxis error at the kth simulation step. This metric is thus the minimal time such that the eigenaxis error in the 100 most recent simulation steps is less than 0.05 rad.

5.1 M2R Examples without Disturbances

To illustrate the inertia-free property of the control laws, the inertia of the spacecraft is varied using

$$J_{ij}(\alpha) = (1-\alpha)J_i + \alpha J_j, \tag{23}$$

where $\alpha \in [0, 1]$ for $i, j \in \{(1, 5), (3, 1), (3, 5), (3, 4)\}$.

Next, we examine the robustness of the thrusters to misalignment relative to the principal axes. To model this misalignment, the inertia matrix is rotated by an angle θ about either the x-axis, y-axis, or z-axis. For each rotation, J_3 is transformed by

$$J_3' = \mathcal{O}(\theta)J_3\mathcal{O}(\theta)^\mathrm{T}, \tag{24}$$

where $\mathcal{O}(\theta)$ is a direction cosine matrix.

Figure 2 shows how the thruster misalignment angle θ affects the settling time, where θ is varied from -180 deg to 180 deg. Figure 2 also shows how the R2R settling time depends on α. Both inertia robustness studies are shown for SO(3)/3 and SO(3)/9.

5.2 M2R Examples with Disturbances

Figure 3 illustrates how the control laws handle body-constant disturbance torques about the minor axis. Note that SO(3)/0 and SO(3)/6 are not able to reject constant torque disturbances.

Next, we consider a gravity gradient disturbance torque τ_{g} modeled by [17, pp. 386–390]

$$\tau_g = 3n^2(\mathcal{O}_{\mathrm{SC/L}}e_3)^{\times} J(\mathcal{O}_{\mathrm{SC/L}}e_3), \tag{25}$$

where $n \triangleq \sqrt{\mu/r^3}$ is the orbital mean motion, μ is the gravitational parameter, r is the orbit radius, e_3 is the third column of the 3×3 identity matrix, and $\mathcal{O}_{\mathrm{SC/L}} \in \mathbb{R}^{3\times 3}$ is the orientation matrix of the spacecraft frame $\mathrm{F_{SC}}$ relative to the local-vertical-local-horizontal frame $\mathrm{F_L}$. The satellite orbit is circular with an altitude of 300 km.

Figure 4 shows that SO(3)/3 and SO(3)/9 can reject gravity gradient disturbances for a R2R maneuver. Furthermore, Figure 5 shows the closed-loop performance of SO(3)/3 and SO(3)/9 for a commanded inertial attitude in the presence of a gravity gradient disturbance.

Next, we consider an inertially constant disturbance torque. Figure 6 shows the performance of all four controllers as the disturbance magnitude is increased. The settling time is computed for the control laws that can reject the inertially constant disturbance, whereas the steady-state error is computed for those that bring the spacecraft to rest with an incorrect attitude.

5.3 M2R Examples with Input Nonlinearities

Next, we consider the effect of three nonlinearities, namely, torque cut-off saturation, control-torque deadzone, and thrusters operating in on-off mode with the input torque given by the on-off control law $u(t) = u_{\max}\mathrm{sign}(v(t))$, where $v(t)$ is the torque commanded by the SO(3) control law. Figure 7 shows the effect of increasingly restrictive saturation levels for all of the control laws. Figure 8 shows how each controller performs the same M2R maneuver using on-off actuation. Figure 9 illustrates how the settling time changes as a function of the width of the unknown control-torque deadzone.

We also consider the effect of sensor noise corrupting the angular-velocity measurement. Two types of noise are considered, namely, gyro bias, that is, a constant error in the measurement of ω, as well as zero-mean white gyro noise with a signal-to-noise ratio of 20. Figure 10 shows the performance of all four controllers when either gyro bias or stochastic gyro noise is present. SO(3)/3, SO(3)/6, and SO(3)/9 are able to reduce the attitude error below 0.05 rad.

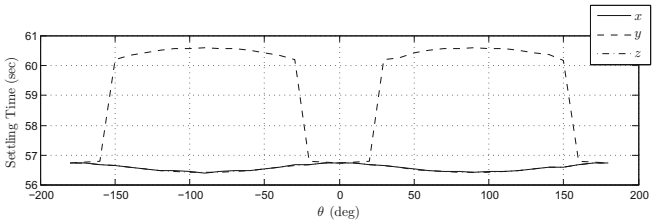

(a) SO(3)/3. Variations in the settling time are within 7%.

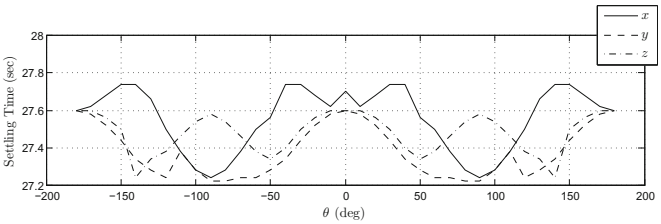

(b) SO(3)/9. Variations in the settling time are within 2%.

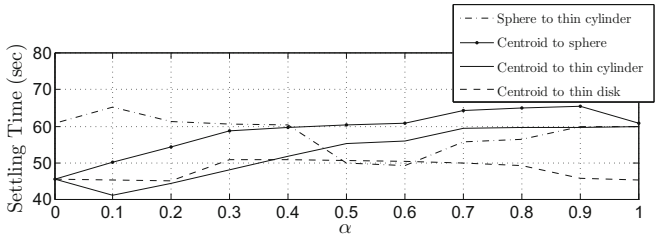

(c) SO(3)/3. Variations in the settling time are within 30%.

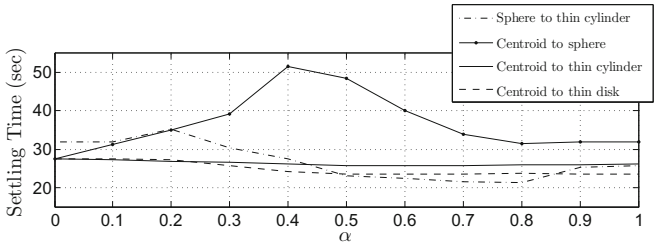

(d) SO(3)/9. Variations in the settling time are within 44%.

Fig. 2. R2R settling time with no disturbance for SO(3)/3 and SO(3)/9 as a function of the principal-frame/body-frame rotation angle θ for misalignments about each of the three principal axes of J_3 (a), (b), and the perturbation parameter α for various combinations of inertia matrices (c), (d). The commanded maneuver is a 40-deg rotation about the body-fixed direction $[1\ 1\ 1]^{\mathrm{T}}$. Each controller is implemented with a single tuning for all inertia cases. Convergence is achieved for all four cases.

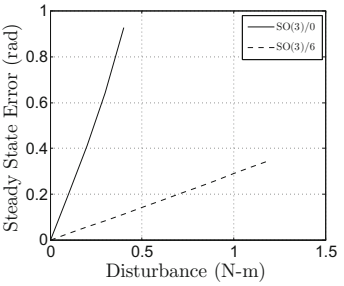

(a) R2R steady-state error for SO(3)/0 and SO(3)/6.

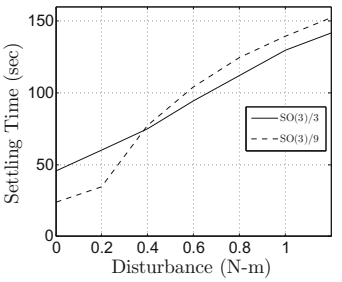

(b) R2R settling time for SO(3)/3 and SO(3)/9.

Fig. 3. Body-constant torque-disturbance rejection about the minor axis. The commanded maneuver is a 40-deg rotation about the body-fixed direction $[1\ 1\ 1]^{\mathrm{T}}$. Note that the performance of SO(3)/6 is substantially better than the performance of SO(3)/0, and the performance of SO(3)/3 improves relative to SO(3)/9 as the magnitude of the torque disturbance increases.

However, SO(3)/0 is not able to achieve the commanded attitude in the presence of either gyro bias or zero-mean white measurement noise.

6 M2S Examples

6.1 M2S Examples without Disturbances

Next, we consider M2S maneuvers. For spins about a principal axis, Euler's equation becomes a linear second-order system, and thus integrators in the controller are not required to stabilize spin commands. As shown in Figure 11, SO(3)/0 can stabilize spins about a principal axis. Figure 12 shows, however, that SO(3)/0 cannot follow spin commands about a non-principal axis.

6.2 M2S Examples with Disturbances

Figure 13 shows that SO(3)/3 and SO(3)/9 can achieve spins about a non-principal axis in the presence of constant torque disturbances.

Figure 14 shows that SO(3)/6 is able to follow spin commands about a non-principal axis, albeit with large settling times. In the presence of a torque disturbance, SO(3)/6 cannot follow spin commands, and the resulting spin is about an incorrect axis. Consistent with [17, pp. 377], Figure 14 also confirms that non-principal-axis spins are unstable, since the spacecraft attitude diverges when the input torque is switched off.

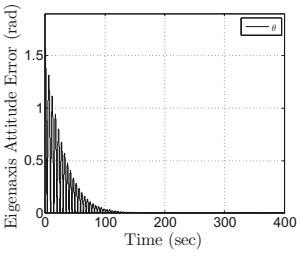

(a) SO(3)/3. Eigenaxis attitude error.

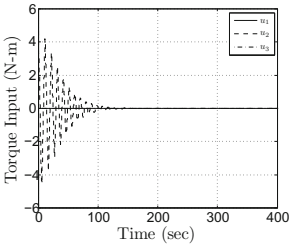

(b) SO(3)/3. Torque input

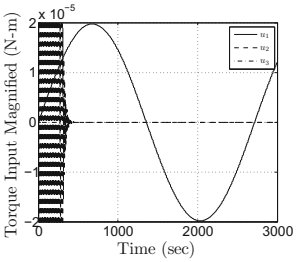

(c) SO(3)/3. Torque input zoomed.

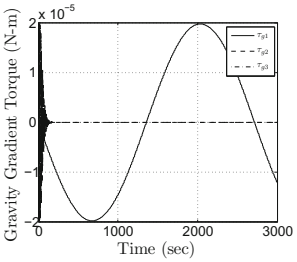

(d) SO(3)/3. Gravity gradient disturbance torque.

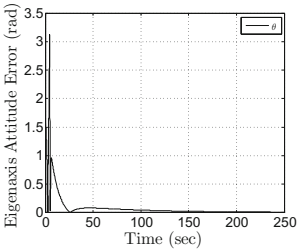

(e) SO(3)/9. Eigenaxis error.

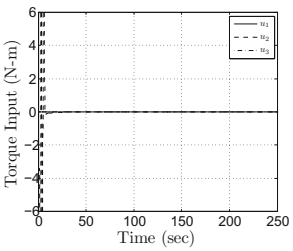

(f) SO(3)/9. Torque input.

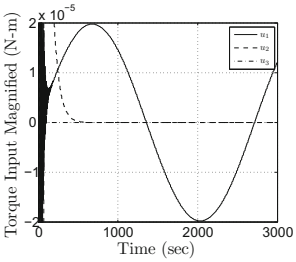

(g) SO(3)/9. Torque input zoomed.

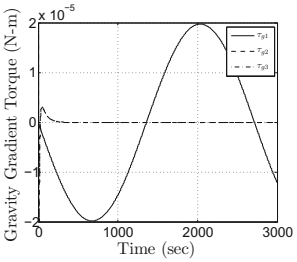

(h) SO(3)/9. Gravity gradient disturbance torque.

Fig. 4. Gravity gradient disturbance rejection for SO(3)/3 and SO(3)/9. The commanded maneuver is a 90-deg rotation about the body-fixed direction $[0\ 1\ 0]^{\mathrm{T}}$. The spacecraft is stabilized, and the disturbance torque is rejected. Note that the control input is the mirror image of the disturbance torque once that the commanded attitude is achieved.

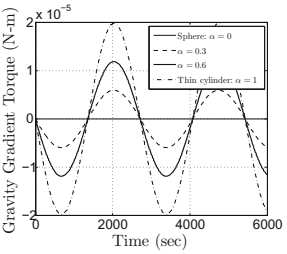

(a) SO(3)/3. Gravity gradient disturbance torque.

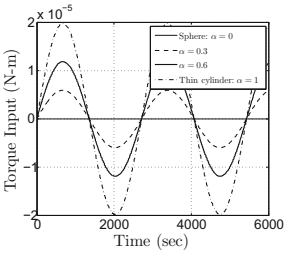

(b) SO(3)/3. Torque input.

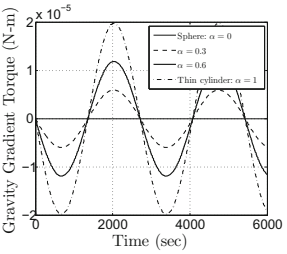

(c) SO(3)/9. Gravity gradient disturbance torque.

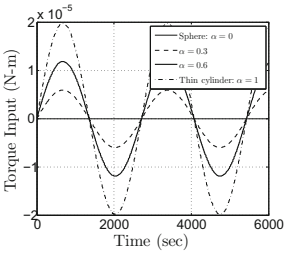

(d) SO(3)/9. Torque input.

Fig. 5. Gravity-gradient disturbance rejection for SO(3)/3 and SO(3)/9. The commanded motion is along a circular orbit with $R(0) = I$ and the commanded attitude $R_{\mathrm{d}} = I$. Note that the inertially constant pointing command is achieved despite the presence of an attitude-dependent sinusoidal disturbance due to gravity gradients. Note that the control input is the mirror image of the disturbance torque.

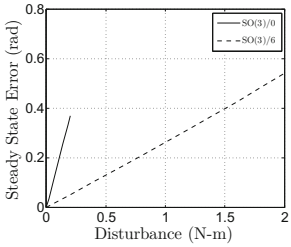

(a) R2R steady-state error for SO(3)/0 and SO(3)/6.

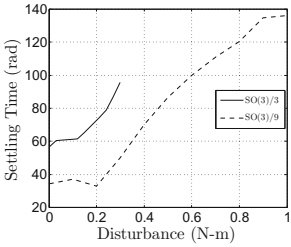

(b) R2R settling time for SO(3)/3 and SO(3)/9.

Fig. 6. Inertially constant disturbance-torque rejection about the inertially fixed direction $[0\ 0\ 1]^{\mathrm{T}}$. The maneuver is a 40-deg rotation about the body-fixed direction $[1\ 1\ 1]^{\mathrm{T}}$. The control laws SO(3)/0 and SO(3)/6 bring the spacecraft to rest with an attitude offset, whereas SO(3)/3 and SO(3)/9 bring the spacecraft to rest with the commanded attitude. Note that SO(3)/6 and SO(3)/9 perform substantially better than SO(3)/0 and SO(3)/3.

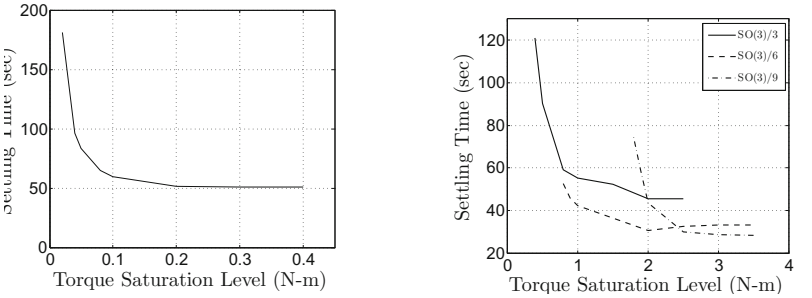

(a) SO(3)/0. (b) SO(3)/3, SO(3)/6, and SO(3)/9.

Fig. 7. R2R settling time as a function of the control-torque saturation level on all three axes. The maneuver is a 40-deg rotation about the body-fixed direction $[1\ 1\ 1]^{\mathrm{T}}$. Note that, at low saturation levels, SO(3)/0 stabilizes the spacecraft, whereas SO(3)/3, SO(3)/6, and SO(3)/9 fail. Saturation does not affect the performance of SO(3)/0 for saturation levels greater than 0.3 N-m.

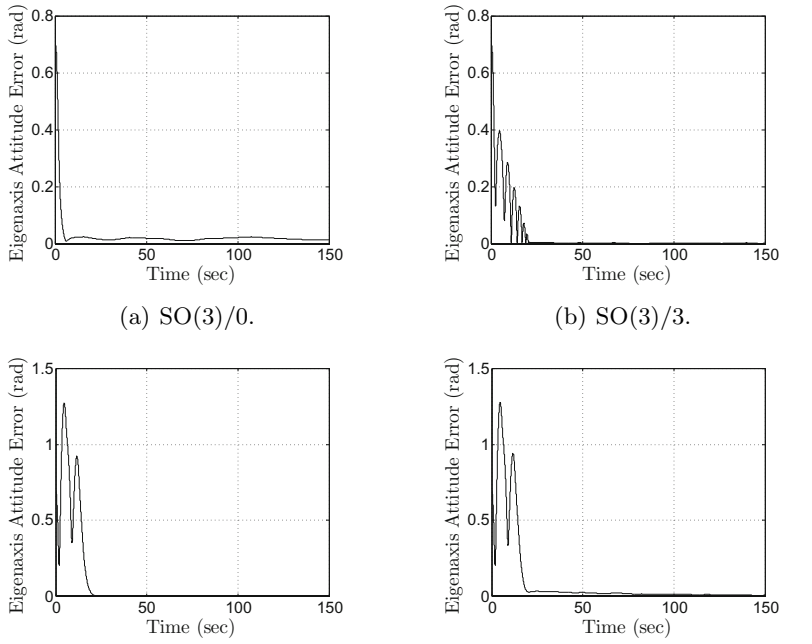

(a) SO(3)/0. (b) SO(3)/3.

(c) SO(3)/6. (d) SO(3)/9.

Fig. 8. Performance comparison using on-off thrusters. The maneuver is a 40-deg rotation about the body-fixed direction $[1\ 1\ 1]^{\mathrm{T}}$. The tuning parameters and control-torque magnitude are the same in all four cases.

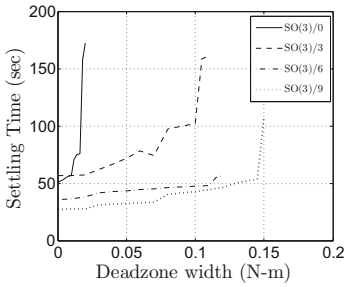

Fig. 9. R2R settling time for all four control laws as a function of the width of an unknown control-torque deadzone. The maneuver is a 40-deg rotation about the body-fixed direction $[1\ 1\ 1]^{\mathrm{T}}$. Note that, for deadzones of small width, SO(3)/0 fails to stabilize the spacecraft, whereas SO(3)/3, SO(3)/6, and SO(3)/9 can stabilize at much higher control-torque deadzones.

7 Comparison to Classical Optimal Control

Classical optimal control laws have been applied extensively to spacecraft rotational maneuvers [20–22]. These control laws are based on the minimum principle, and, unlike the inertia-free SO(3) control laws considered in this paper, they assume exact knowledge of the inertia properties of the spacecraft. Nevertheless, it is useful to compare the performance of these control laws to the SO(3) control laws in order to assess the effect of inertia uncertainty modeling information.

For 3-axis maneuvers, the control laws given in [20–22] involve complicated switching strategies. For simplicity, we therefore assume that the commanded maneuver is about the major axis only, giving double integrator dynamics, and with the direction and moment of inertia of the major axis assumed to be known. Using the classical time-optimal control law

$$u = -u_{\max}\mathrm{sign}\left(\theta - \frac{J}{2u_{\max}}\dot{\theta}|\dot{\theta}|\right), \tag{26}$$

where $u_{\max} > 0$ is the control-torque magnitude and θ is the rotation angle about the major axis, we simulate the closed-loop system and compare the settling time to that of the SO(3) control laws operating in on-off mode with the same magnitude as (26). Note that the inertia in (26) is the true spacecraft inertia. To determine the performance of (26) under imperfect modeling information, we then introduce uncertainty about both the major moment of inertia and the direction of the major axis. Comparisons with the SO(3) control laws provide a baseline tradeoff between settling time and modeling accuracy. The results of these comparisons are shown in Figures 15 and 16.

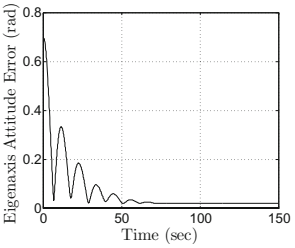

(a) SO(3)/0. Gyro bias.

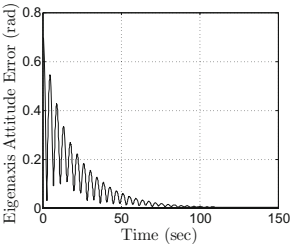

(b) SO(3)/3. Gyro bias.

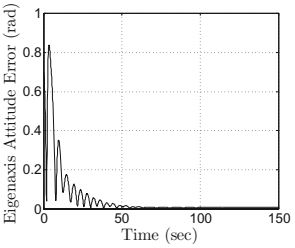

(c) SO(3)/6. Gyro bias.

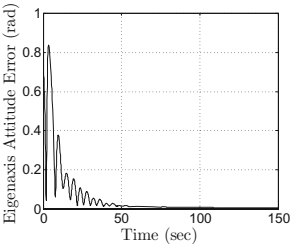

(d) SO(3)/9. Gyro bias.

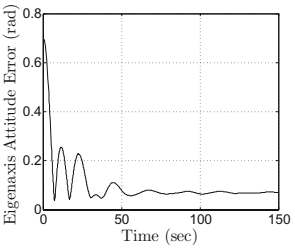

(e) SO(3)/0. Zero-mean white gyro measurement noise.

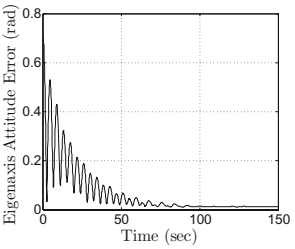

(f) SO(3)/3. Zero-mean white gyro measurement noise.

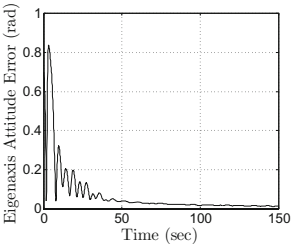

(g) SO(3)/6. Zero-mean white gyro measurement noise.

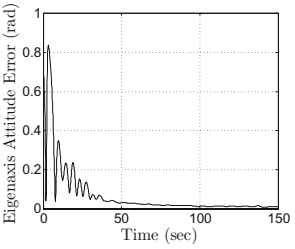

(h) SO(3)/9. Zero-mean white gyro measurement noise.

Fig. 10. (a)–(d) Controller performance in the presence of a gyro bias of $[0\ 0\ 0.01]^{\mathrm{T}}$ rad/sec. (e)–(h) Comparison of controller sensitivity to zero-mean white gyro measurement noise with a signal-to-noise ratio of 20. All four controllers are able to bring the spacecraft to rest. However, SO(3)/0 is not able to stabilize to the correct attitude with either gyro bias or white noise. In all simulations, the maneuver is a 40-deg rotation about the body-fixed direction $[1\ 1\ 1]^{\mathrm{T}}$. The tuning parameters and signal-to-noise ratio are kept the same.

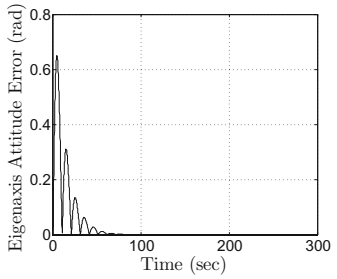

(a) Eigenaxis error.

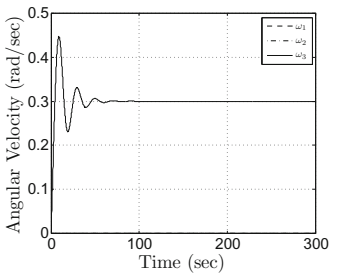

(b) Angular velocity components.

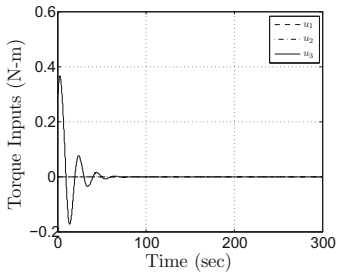

(c) Torque inputs.

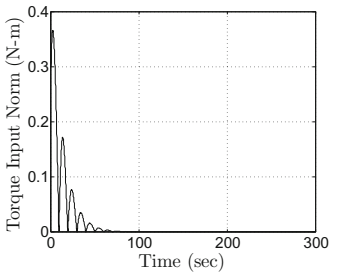

(d) Torque input 2-norm.

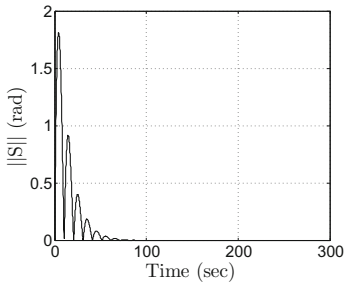

(e) 2-norm of S.

Fig. 11. R2S maneuver for SO(3)/0 with $\omega_{\mathrm{d}} = [0\ 0\ 0.3]^{\mathrm{T}}$ rad/sec. The spacecraft is initially at rest with $R = I$ and $R_{\mathrm{d}}(0) = I$. The controller is able to follow the spin command, which is about a principal axis.

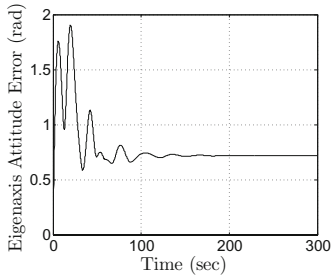

(a) Eigenaxis error.

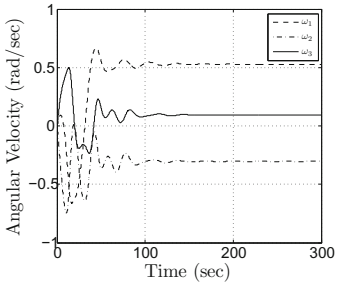

(b) Angular velocity components.

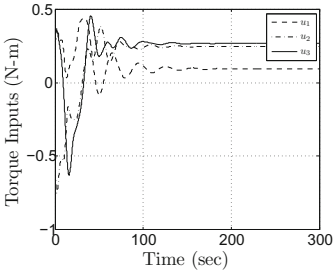

(c) Torque inputs.

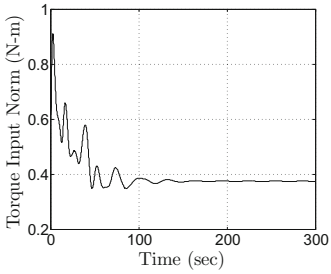

(d) Torque input 2-norm.

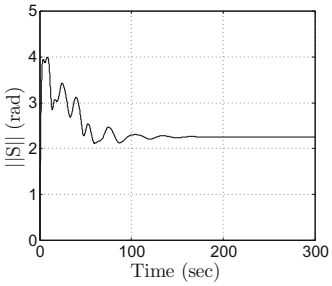

(e) 2-norm of S.

Fig. 12. R2S maneuver for SO(3)/0 with $\omega_{\rm d} = [0.2\ -0.5\ \ 0.3]^{\rm T}$ rad/sec. The spacecraft is initially at rest with $R = I$ and $R_{\rm d}(0) = I$. The controller spins the spacecraft with the commanded angular rate but about an incorrect axis, as shown by the attitude error. Thus SO(3)/0 cannot follow the spin command, which is about a non-principal axis.

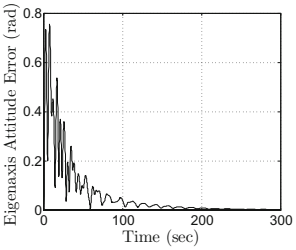

(a) SO(3)/3. Eigenaxis error.

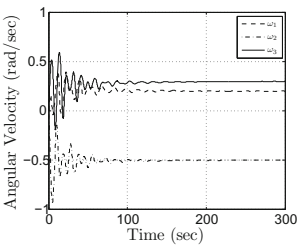

(b) SO(3)/3. Angular velocity components.

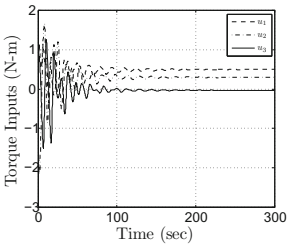

(c) SO(3)/3. Torque inputs.

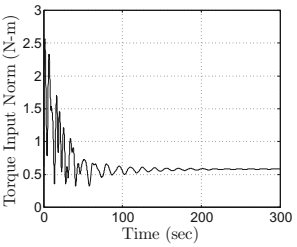

(d) SO(3)/3. Torque input 2-norm.

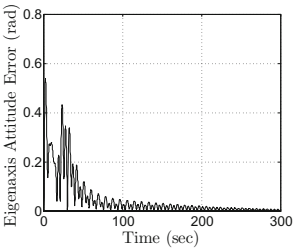

(e) SO(3)/9. Eigenaxis error.

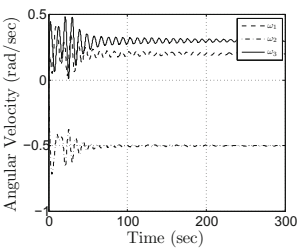

(f) SO(3)/9. Angular velocity components.

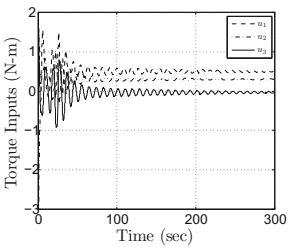

(g) SO(3)/9. Torque inputs.

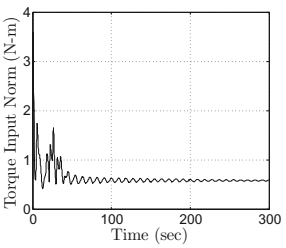

(h) SO(3)/9. Torque input 2-norm.

Fig. 13. R2S maneuver for $\omega_{\mathrm{d}} = [0.2\ -0.5\ \ 0.3]^{\mathrm{T}}$ rad/sec with gravity gradient disturbance and the body-constant disturbance torque $d = [0\ 0\ 0.2]^{\mathrm{T}}$ N-m for SO(3)/3 and SO(3)/9. The spacecraft is initially at rest with $R = I$ and $R_{\mathrm{d}}(0) = I$. The controller rejects the disturbances and follows the spin command.

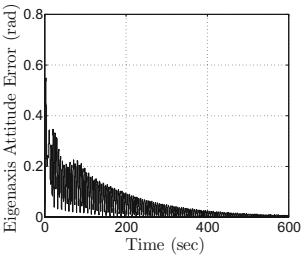

(a) SO(3)/6. Eigenaxis error.

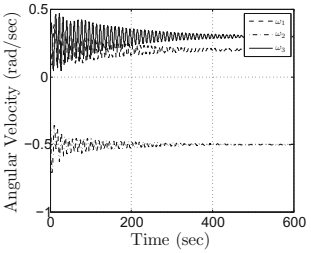

(b) SO(3)/6. Angular velocity.

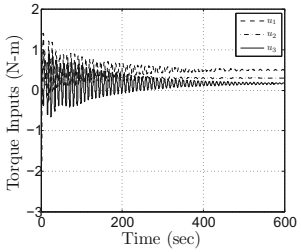

(c) SO(3)/6. Torque inputs.

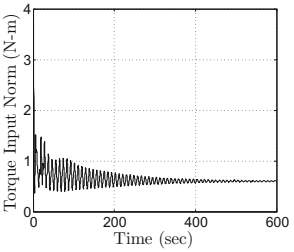

(d) SO(3)/6. Torque input norm.

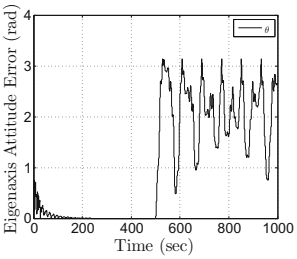

(e) SO(3)/3. Eigenaxis error.

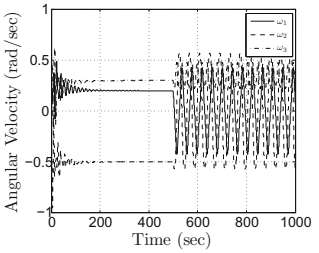

(f) SO(3)/3. Angular velocity.

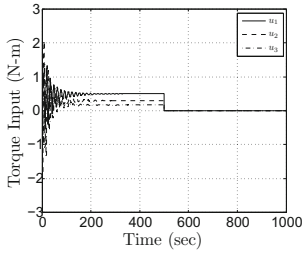

(g) SO(3)/3. Torque inputs.

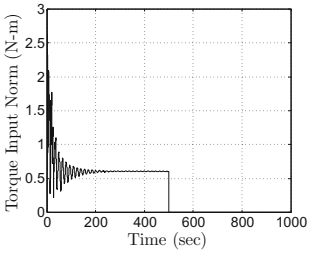

(h) SO(3)/3. Torque input norm.

Fig. 14. R2S maneuver for SO(3)/6 and SO(3)/3 with $\omega_{\rm d} = [0.2\ -0.5\ \ 0.3]^{\rm T}$ rad/sec. The spacecraft is initially at rest with $R = I$ and $R_{\rm d}(0) = I$. The controllers follow the spin command. In the case of SO(3)/3, the torque input is switched off at time $t = 500$ sec to show the instability of the commanded spin about a non-principal axis.

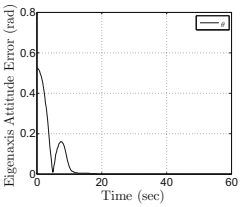

(a) SO(3)/0 control law.

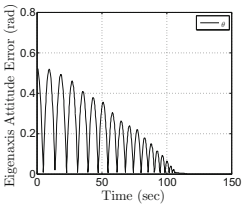

(b) SO(3)/3 control law.

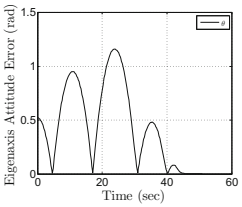

(c) SO(3)/6 control law.

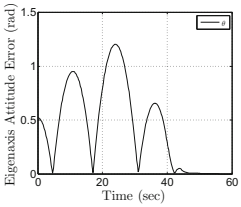

(d) SO(3)/9 control law.

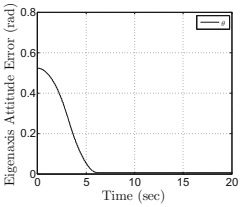

(e) Bang-bang control law.

Fig. 15. Convergence-time comparison for the SO(3) control laws using on-off thrusters and the classical optimal bang-bang control law. The maneuver is a 30-deg rotation about the body-fixed principal-axis direction $[1\ 0\ 0]^{\mathrm{T}}$. The torque on-level $u_{\max} = 0.5$ N-m is the same for all controllers. The inertia used in the optimal bang-bang control law is the true spacecraft inertia J.

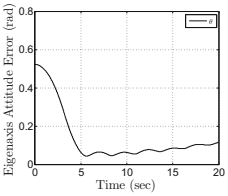

(a) Eigenaxis error.

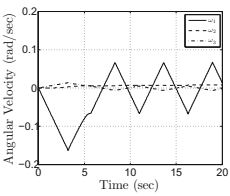

(b) Angular velocity.

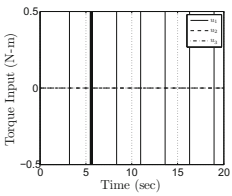

(c) Torque input.

Fig. 16. Performance of the classical optimal bang-bang control law in the presence of an inertia error. The actual bang-bang inertia matrix is rotated relative to the true spacecraft inertia matrix. This inertia misalignment is a 5-deg rotation about the body-fixed direction $[0\ 1\ 0]^{\mathrm{T}}$. The commanded maneuver is a 30-deg rotation about the body-fixed direction $[1\ 0\ 0]^{\mathrm{T}}$. Note that a slight inertia misalignment leads to failure of the bang-bang control law.

Table 2. Summary of controller capabilities. Motion to rest (M2R), gravity gradient disturbances (GG), constant torque disturbance (in body frame) (BD), constant torque disturbance (in inertial frame) (ID), torque saturation level (SAT), unknown control-torque deadzone (DZ), and on-off thruster actuation (ON/OFF). The notation used is, Y, N: Yes or no; L, S: based on Lyapunov theory or based on simulation.

Maneuver	SO(3)/0	SO(3)/3	SO(3)/6	SO(3)/9
M2R	Y/L	Y/S	Y/S	Y/L
M2R + ID	N/S	Y/S	N/S	Y/L
M2R + GG + BD	N/S	Y/S	N/S	Y/L
M2R + SAT	Y/S	Y/S	Y/S	Y/S
M2R + DZ	Y/S	Y/S	Y/S	Y/S
M2R + ON/OFF	Y/S	Y/S	Y/S	Y/S
M2R + GYRO BIAS	N/S	Y/S	Y/S	Y/S
M2R + WHITE NOISE	N/S	Y/S	Y/S	Y/S
M2S	N/S	Y/S	Y/S	Y/L
M2S + BD	N/S	Y/S	N/S	Y/L
M2S + SAT	N/S	Y/S	Y/S	Y/S

8 Conclusions

We compared four inertia-free PID-type spacecraft attitude control laws (SO(3)/0, SO(3)/3, SO(3)/6, SO(3)/9) under M2R and M2S command scenarios with various types of disturbances. All four controllers are able to achieve M2R and M2S around a principal axis in the absence of disturbances. In addition, SO(3)/3 and SO(3)/9 can achieve M2R and M2S in the presence of inertially constant and body-constant disturbances, and M2R in the presence of inertially time-varying disturbances around both principal and non-principal axes. Note that SO(3)/3 needs six fewer integrators than SO(3)/9, although SO(3)/9 achieves the commanded motion in less time.

Furthermore, all four controllers achieve M2R in the presence of torque saturation. For this objective, SO(3)/0 can stabilize the spacecraft with a significantly lower level of saturation than SO(3)/3, SO(3)/6, and SO(3)/9. For M2S maneuvers, SO(3)/0 is not effective, although SO(3)/3, SO(3)/6, and SO(3)/9 are effective for arbitrary spin axes. Table 2 summarizes the cases for which each SO(3) control law is able or not able to achieve the commanded maneuver.

For an unknown control-torque deadzone nonlinearity, we found that SO(3)/6 and SO(3)/9 are less sensitive to this nonlinearity. For on-off control torques, SO(3)/3 is the most accommodating. We also compared performance when sensor noise is present. In this case, SO(3)/3, SO(3)/6, and SO(3)/9 can stabilize M2R maneuvers despite gyro bias or white noise.

Future research will focus on a Lyapunov foundation for SO(3)/3 as well as extensions to spacecraft with wheels. Preliminary results are given in [19, 23].

References

1. Junkins, J.L., Akella, M.R., Robinett, R.D.: Nonlinear Adaptive Control of Spacecraft Maneuvers. AIAA J. Guid. Contr. Dyn. 20, 1104–1110 (1997)
2. Egeland, O., Godhavn, J.M.: Passivity-Based Adaptive Attitude Control of a Rigid Spacecraft. IEEE Transactions on Automatic Control 39, 842–846 (1994)
3. Ahmed, J., Coppola, V.T., Bernstein, D.S.: Asymptotic Tracking of Spacecraft Attitude Motion with Inertia Identification. AIAA J. Guid. Contr. Dyn. 21, 684–691 (1998)
4. Wen, J.T.Y., Kreutz-Delgado, K.: The Attitude Control Problem. IEEE Transactions on Automatic Control 36, 1148–1162 (1991)
5. Bhat, S.P., Bernstein, D.S.: A Topological Obstruction to Continuous Global Stabilization of Rotational Motion and the Unwinding Phenomenon. Sys. Contr. Lett. 39, 63–70 (2000)
6. Wie, B., Barba, P.M.: Quaternion Feedback for Spacecraft Large Angle Maneuvers. AIAA J. Guid. Contr. Dyn. 8, 360–365 (1985)
7. Joshi, S.M., Kelkar, A.G., Wen, J.T.: Robust Attitude Stabilization Using Nonlinear Quaternion Feedback. IEEE Trans. Autom. Contr. 40, 1148–1161 (1995)
8. Crassidis, J.L., Vadali, S.R., Markley, F.L.: Optimal Variable-Structure Control Tracking of Spacecraft Maneuvers. AIAA J. Guid. Contr. Dyn. 23, 564–566 (2000)
9. Mayhew, C.G., Sanfelice, R.G., Teel, A.R.: Quaternion-Based Hybrid Control for Robust Global Attitude Tracking. IEEE Trans. Autom. Contr. 56, 2555–2566 (2011)
10. Chaturvedi, N., Sanyal, A.K., McClamroch, N.H.: Rigid Body Attitude Control: Using Rotation Matrices for Continuous, Singularity-free Control Laws. IEEE Contr. Sys. Mag. 31(3), 30–51 (2011)
11. Koditschek, D.E.: The Application of Total Energy as a Lyapunov Function for Mechanical Control Systems. In: Proc. AMS-IMS-SIAM Joint Summer Research Conference, AMS Dynamics and Control of Multibody Systems, pp. 131–157 (1988)
12. Chaturvedi, N.A., McClamroch, N.H., Bernstein, D.S.: Asymptotic Smooth Stabilization of the Inverted 3D Pendulum. IEEE Trans. Automa. Contr. 54, 1204–1215 (2009)
13. Chaturvedi, N.A., McClamroch, N.H., Bernstein, D.S.: Stabilization of a 3D Axially Symmetric Pendulum. Automatica 44, 2258–2265 (2008)
14. Chaturvedi, N.A.: Global Dynamics and Stabilization of Rigid Body Attitude Systems. PhD thesis, University of Michigan, Ann Arbor, MI (2007)
15. Sanyal, A., Fosbury, A., Chaturvedi, N., Bernstein, D.S.: Inertia-Free Spacecraft Attitude Tracking with Disturbance Rejection and Almost Global Stabilization. AIAA J. Guid. Contr. Dyn. 32, 1167–1178 (2009)
16. Bullo, F., Lewis, A.D.: Geometric Control of Mechanical Systems. Springer (2005)
17. Wie, B.: Space Vehicle Dynamics and Control, vol. 2. AIAA (2008)
18. Cruz, G., Yang, X., Weiss, A., Kolmanovsky, I., Bernstein, D.S.: Torque-saturated, Inertia-free Spacecraft Attitude Control. AIAA–2011–6507 (August 2011)
19. Weiss, A., Kolmanovsky, I., Bernstein, D.S., Sanyal, A.: Inertia-Free Spacecraft Attitude Control Using Reaction Wheels. AIAA J. Guid. Contr. Dyn. 36, 1425–1439 (2013)
20. Junkins, J.L., Turner, J.D.: Optimal Spacecraft Rotational Maneuvers. Elsevier, Amsterdam (1986)
21. Bai, K.D., Wie, B.: Time-Optimal Three-Axis Reorientation of a Rigid Spacecraft. AIAA J. Guid. Contr. Dyn. 16, 446–452 (1993)

22. Bai, X., Junkins, J.L.: New Results for Time-Optimal Three-Axis Reorientation of a Rigid Spacecraft. AIAA J. Guid. Cont. Dyn. 32, 1071–1076 (2009)
23. Agarwal, K., Weiss, A., Kolmanovsky, I., Bernstein, D.S.: Inertia-Free Spacecraft Attitude Control with Control-Moment-Gyro Actuation. In: Proc. AIAA Guid. Nav. Contr. Conf. AIAA-2012-5003-282 (August 2012)